catalysts

MDPI

Article

Bifunctional CuO-Ag/KB Catalyst for the Electrochemical Reduction of CO_2 in an Alkaline Solid-State Electrolysis Cell

Sabrina Campagna Zignani *, Massimiliano Lo Faro, Alessandra Palella, Lorenzo Spadaro, Stefano Trocino, Carmelo Lo Vecchio and Antonino Salvatore Aricò

CNR-ITAE, Istituto di Tecnologie Avanzate per l'Energia "Nicola Giordano", Via Salita S. Lucia sopra Contesse 5, 98126 Messina, Italy; lofaro@itae.cnr.it (M.L.F.); palella@itae.cnr.it (A.P.); spadaro@itae.cnr.it (L.S.); trocino@itae.cnr.it (S.T.); lovecchio@itae.cnr.it (C.L.V.); arico@itae.cnr.it (A.S.A.)

* Correspondence: zignani@itae.cnr.it

Abstract: The conversion of carbon dioxide into value-added products is progressively gaining momentum. Several strategies have been used to develop technologies that reduce the net emissions of CO_2. The utilisation of CO_2 could either contribute to carbon recycling. In this paper, the transformation of CO_2 was investigated in a coelectrolysis cell constituted of a solid polymer electrolyte, a carbon-supported CuO-Ag composite cathode and NiFeOx anode. Noncritical raw materials were synthesised according to the oxalate method and investigated in an alkaline environment. Low-carbon alcohols were obtained with a specific selectivity for ethanol and methanol over the CuO-Ag/KB cathode. The reaction rates at 1.6 V and 1.8 V cell voltages have been determined in steady-state experiments using $NaHCO_3$ supporting electrolyte recirculated at the anode.

Keywords: renewables; CO_2 reduction; zero-gap electrochemical cell; synthetic alcohols; CRM-free catalyst

Citation: Zignani, S.C.; Lo Faro, M.; Palella, A.; Spadaro, L.; Trocino, S.; Lo Vecchio, C.; Aricò, A.S. Bifunctional CuO-Ag/KB Catalyst for the Electrochemical Reduction of CO_2 in an Alkaline Solid-State Electrolysis Cell. *Catalysts* **2022**, *12*, 293. https://doi.org/10.3390/catal12030293

Academic Editor: Jianping Yang

Received: 20 January 2022
Accepted: 2 March 2022
Published: 4 March 2022

1. Introduction

The electrochemical reduction of CO_2 to produce green chemicals is an attractive approach for storing renewable energy and mitigating net greenhouse gas emissions in the atmosphere [1–8]. The conversion of CO_2 is, in principle, prohibitive in conventional electrolysers based on a concentrated liquid alkaline electrolyte due to its immediate reaction to form a salt [9–11]. However, novel and advanced electrolysers based on solid-state alkaline electrolytes can become a promising technology for this process, although they still need to solve the high cost of materials and their durability [10,12]. Resistance to the CO_2 environment of polymeric electrolytes with anionic functional groups is still under study, whereas the maximum operating temperature is 60 °C for most alkaline membranes developed until now [13–18]. Recent encouraging results in this field have fuelled the investigation of novel and hierarchical materials based on non-noble and noncritical raw materials, which generally are not stable in an acidic environment [9,19,20]. In principle, the electrodes based on noncritical raw materials (CRMs-free) are less effective than precious metal catalysts [21,22]. At the same time, the alkaline environment enhances the oxygen evolution kinetics due to the lower energy required compared to that in the acidic conditions, and the CO_2 solubility producing an enhancement of the reaction rate according to the specific reaction order. Particular disadvantages of alkaline electrolytes include lower ionic conductivity than H^+-based electrolytes and the need to recirculate caustic solutions [12,23,24]. However, in the absence of a breakthrough solution for a cost-effective anode electrocatalyst capable of operation in a protonic environment, i.e., a non-noble metal catalyst sufficiently active and stable at low pH values, the use of alkaline electrolysers, remains the most realistic approach.

This paper investigates the electrochemical reduction of carbon dioxide to alcohols carried out at a cathode based on (CRM-free). The reactions associated with the reduction of

CO_2 to form methanol and ethanol in alkaline conditions and related reversible potentials are presented in following:

$$CO_2 + 5H_2O + 6e^- \rightarrow CH_3OH + 6OH^- \quad E°rev, cathode = 0.04 V vs. RHE \quad (1)$$

$$6OH^- \rightarrow 3/2O_2 + 3H_2O + 6e^- \quad E°rev, anode = 1.225 V vs. RHE \quad (2)$$

$$CO_2 + 2H_2O \rightarrow CH_3\,OH + 3/2O_2 \quad E°rev, cell = 1.185 V \quad (3)$$

$$2CO_2 + 9H_2O + 12e^- \rightarrow CH_3CH_2OH + 12OH^- \quad E°rev, cathode = 0.09 V vs. RHE \quad (4)$$

$$12OH^- \rightarrow 3O_2 + 6H_2O + 12e^- \quad E°rev, anode = 1.225 V vs. RHE \quad (5)$$

$$2CO_2 + 3H_2O \rightarrow CH_3CH_2OH + 3O_2 \quad E°rev, cell = 1.135 V \quad (6)$$

Moreover, under operating conditions, different parallel catalytic and electrocatalytic reactions can occur in the cathode chamber [1,9], and these include the formation of CO (4) and formate (5), H_2 evolution (6) and CO reduction (7), which decrease the overall selectivity and yield to methanol.

$$CO_2 + H_2O + 2e^- \rightarrow CO + 2OH^- \quad E°rev, cathode = -0.1 V vs. RHE \quad (7)$$

$$CO_2 + H_2O + 2e^- \rightarrow HCOO^- + OH^- \quad E°rev, cathode = -0.02 V vs. RHE \quad (8)$$

$$2H_2O + 2e^- \rightarrow H_2 + 2OH^- \quad E°rev, cathode = 0.00 V vs. RHE \quad (9)$$

$$CO + 4H_2 \rightarrow CH_3OH \quad (10)$$

In particular, we have studied the role of Ag in combination with the CuO for the cathodic reaction involving CO_2 reduction. The CuO-Ag catalyst was selected to promote a synergistic effect between the copper oxide (usually recognised as one of the most active phases for CO_2 conversion [25,26]) and Ag (a well-known catalyst for CO_2 reduction into CO [8,27,28]). Then, the variable reducing conditions occurring at the cathode during dynamic operation can promote the formation of different species of Cu, including cuprite (Cu_2O). However, a further cathode reduction can form metallic copper, especially under poor enthalpy efficiency. As a parallel reaction, the simultaneous evolution of hydrogen is possible. Ag can effectively mitigate the H_2 evolution reaction, which can be competitive with the methanol yielding by enhancing CO_2 reduction. According to these premises, this study investigates various operating conditions using a complete alkaline CO_2-H_2O coelectrolysis cell [29–32].

2. Results and Discussion

A preliminary study to detect phase purity and morphology was conducted on the milled catalyst. Figure 1 shows the crystal reflection of Ag/KB and CuO-Ag/KB specimens for comparison and includes the typical patterns of CuO (JCPDS card n° 05-0661) and metallic Ag for reference (JCPDS card n° 04-0783). The XRD spectra did not show any phase impurities, and the crystallite sizes determined using the Scherrer equation applied on the FWHM of CuO and Ag peaks were 8 nm and 17 nm, respectively [8,33,34].

We carried out the microscopic analyses to highlight the grain size of CuO and the morphology of the electrocatalyst. As shown in Figure 2, CuO has an oblong aspect and is evenly distributed with a particle size of about 17 nm, confirming the dimension determined through the XRD (Figure 1) and informing about a low agglomeration between the CuO crystallites.

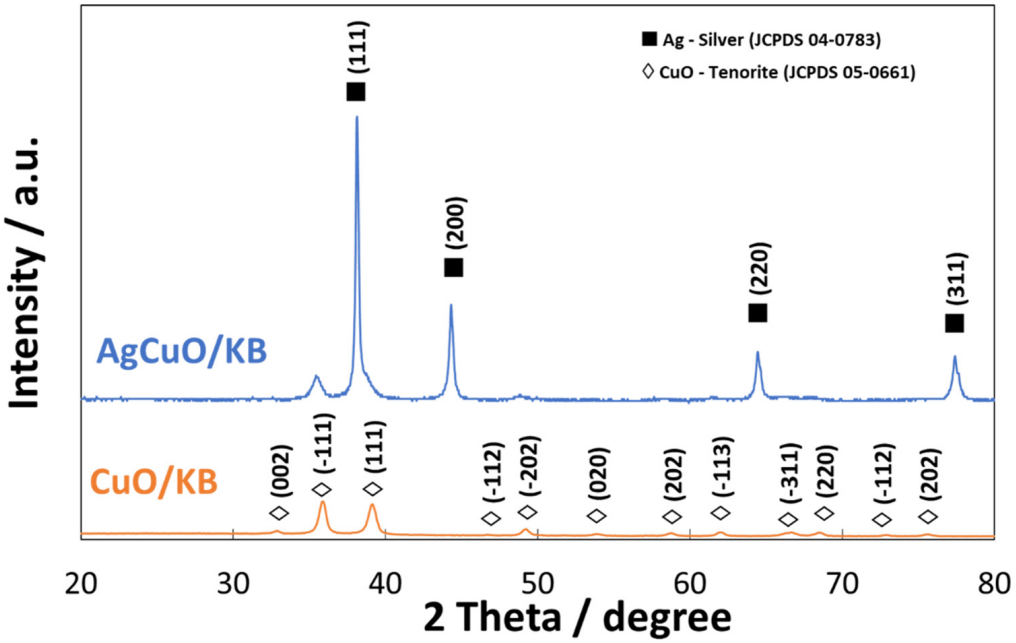

Figure 1. XRD pattern of the CuO-Ag/KB catalyst and CuO/KB catalyst.

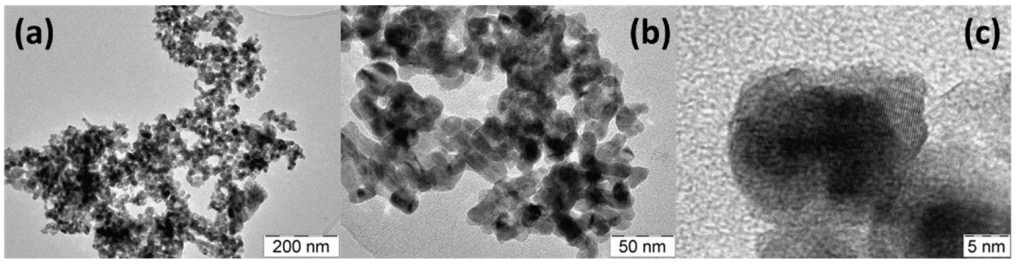

Figure 2. TEM images of the CuO/KB catalyst at three different magnifications. (**a**) 200nm; (**b**) 50 nm; (**c**) 5 nm.

The morphological aspects and chemical analysis of the as milled electrocatalyst are shown in Figure 3. We observed a regular distribution of the two phases, and the EDX analyses confirmed the nominal composition of the as-prepared catalyst.

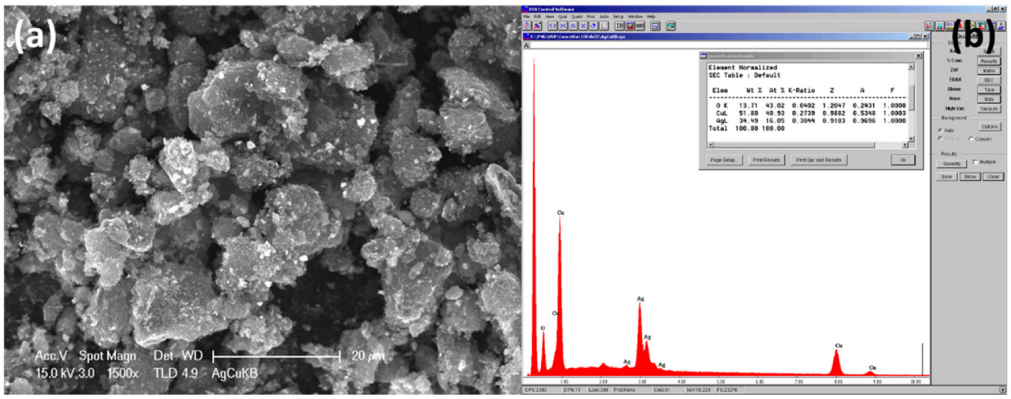

Figure 3. SEM (**a**) and EDX (**b**) analyses of the as-prepared CuO-Ag/KB electrocatalyst.

The analyses of the catalyst surface carried out by XPS analysis revealed an atomic composition of 0.6% silver, 7.7% copper, 8.0% oxygen, carbon as balance, reflecting a low content of Ag in the surface (i.e., Ag:Cu ratio was about 0.1). In Figure 4, the spectra

of C1s, O1s, Cu2p and Ag3d core levels are reported. The spectrum of Cu2p (Figure 4a) consisted of two spin-orbit components at binding energies of 934.4 eV (2p3/2) and 954.6 eV (2p1/2) and two Cu^{2+} shake-up satellites. The shape of the spectrum and the peak positions denotes the presence of Cu(II) species at the surface of CuOxAg/KB system, which are consistent with the structure of cupric oxide (CuO) [35–37]. The binding energy position of Ag 3d5/2 (368.6 eV) and 3d3/2 (374.6 eV) core levels (Figure 4b) proves the valence state of "zero" of the metal (Ag0) [38] at the surface of the catlyst. The profiles of O1s core level of the sample, as reported in Figure 4c, exhibits two components at 530.2 (OI) and 531.9 eV (OII), that can be ascribed to O^{2-} ions of the surface lattice oxygen of CuO and to surface hydroxyl groups (e.g., Cu-OH), respectively [35,37]. The C1s spectrum (Figure 4d) is dominated by the presence of a sharp peak at 284.8 eV, which is typical for carbonaceous solids with a graphite-like surface, such as carbon fibres and graphitized carbon nanospheres [39]. However, the asymmetry of the peak and a small shoulder at higher binding energies, probably ascribable as a weak π–π* interaction, are consistent with the structure of conductive carbon black materials with different surface graphitic characters [40].

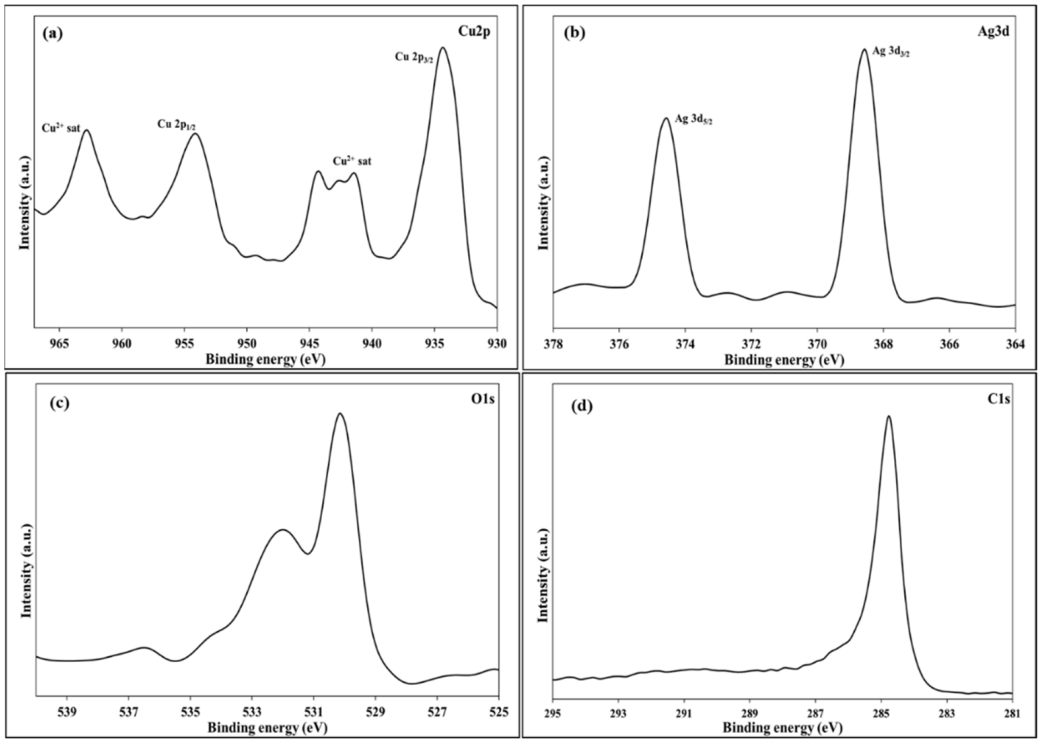

Figure 4. XPS spectra of (**a**) Cu2p, (**b**) Ag3d, (**c**) O1s and (**d**) C1s core levels of CuOxAg/KB catalyst.

Figure 5 provides a scheme of the electrochemical process used for CO_2-H_2O coelectrolysis operating under an alkaline environment. In principle, water should be supplied to the cathode. However, for practical purposes, water containing KOH or $NaHCO_3$ was fed to the anode to avoid diluting the organic products formed at the cathode. An anion exchange membrane separator was used between the CuO-Ag/KB and NiFe-oxide to create a zero-gap cell configuration.

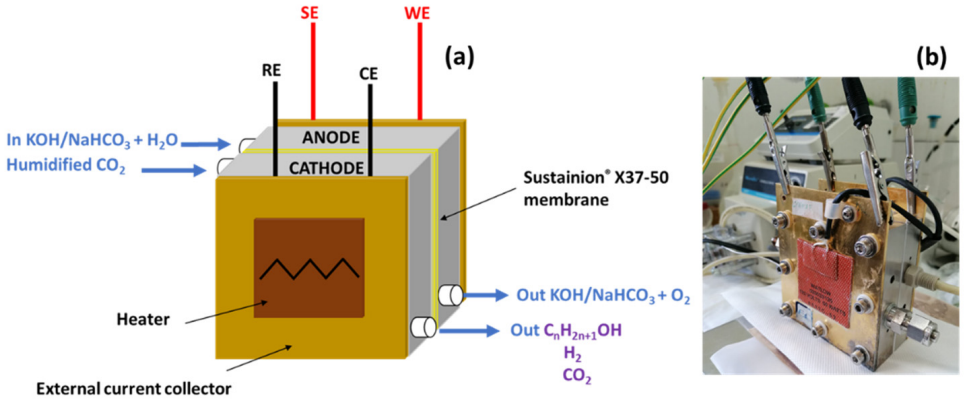

Figure 5. Scheme of the electrochemical process used for CO_2-H_2O coelectrolysis (**a**), single-cell unit (**b**).

The high voltage efficiency range was explored in this study (i.e., a cell voltage < 2 V). The operation at a cell voltage higher than 2 V means significant dissipation of electrical energy and exacerbation of electrochemical corrosion and modification of the cathode catalyst (e.g., reduction of copper oxide to metallic copper). Operation at low potentials combines high voltage efficiency and better stability for the electrocatalysts. Gas-chromatography was used to quantify the liquid phase products. In the first experiments, the characteristics of a MEA based only on CuO at the cathode were investigated. Figure 6 shows the polarisation curves and chronoamperometric test at 1.6 and 1.8 V. Initially, the pure copper oxide catalyst (without Ag) was investigated in the presence of 0.1 M of $NaHCO_3$ at the anode, and humidified CO_2 supplied at the cathode. Potentiostatic tests were carried out at 1.6 (Figure 6b) and 1.8 V (Figure 6d) for 24 h, and the productivity results are reported in Table 1.

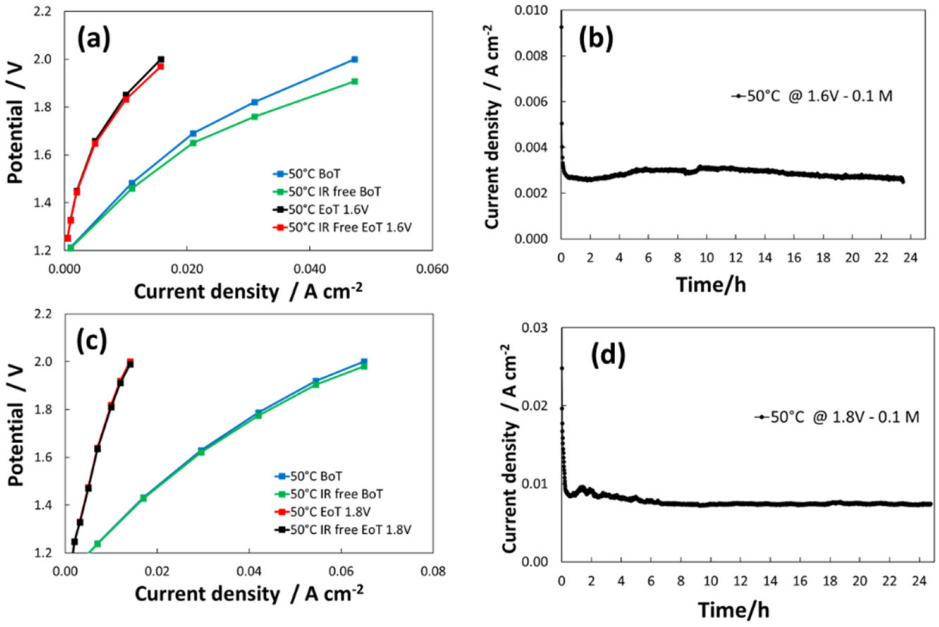

Figure 6. (**a**) Raw and IR-free polarisation curves before (BoT) and after (EoT) a potentiostatic test at 1.6 V. (**b**) Potentiostatic test at 1.6 V/cell. (**c**) Raw and IR-free polarisation curves before (BoT) and after (EoT) a potentiostatic test at 1.8 V. (**d**) Potentiostatic test at 1.8 V/cell. Cell-based on CuOx – Sustainion-NiFeOx, CO_2 feed at the cathode, 0.1 M $NaHCO_3$ feed at the anode.

Table 1. Liquid-phase analysis for cell-based on CuO_x/KB - Sustainion X37-50 -$NiFeO_x$/KB.

CuOx/KB-Sustanion-NiFeOx/KB			
Operative Conditions	**Product Yield (μmol g_{cat}^{-1})**		**CO_2 Conversion Rate (μmol g_{cat}^{-1} h^{-1})**
	Methanol	**Ethanol**	
Cathode CO_2 (50 °C) Anode: 0.1 M $NaHCO_3$ −1.8 V	29.5	14.4	2.43
Cathode CO_2 (50 °C) Anode: 0.1 M $NaHCO_3$ −1.6 V	17.6	9.5	1.52
Cathode CO_2 (50 °C) Anode: 0.5 M $NaHCO_3$ −1.8 V	4.5	0.7	1.19
Cathode CO_2 (50 °C) Anode: 0.5 M $NaHCO_3$ −1.6 V	11.4	7.1	1.07

Polarisation curves indicated substantial activation losses, which are much more relevant after the potentiostatic steady-state operation indicating a poisoning effect by CO_2 adsorption on the electrode surface. The steady-state current density achieved at 1.8 V is 10 mA cm^{-2}. A higher current density and alcohol yield were achieved using 0.1 M $NaHCO_3$ instead of 0.5 M $NaHCO_3$ (Figure 7) probably due to strong adsorption of carbonates on the electrode surface causing a significant poisoning effect. Ohmic resistances are higher in 0.1 M vs. 0.5 M $NaHCO_3$. However, this does not affect the performance at these low current densities.

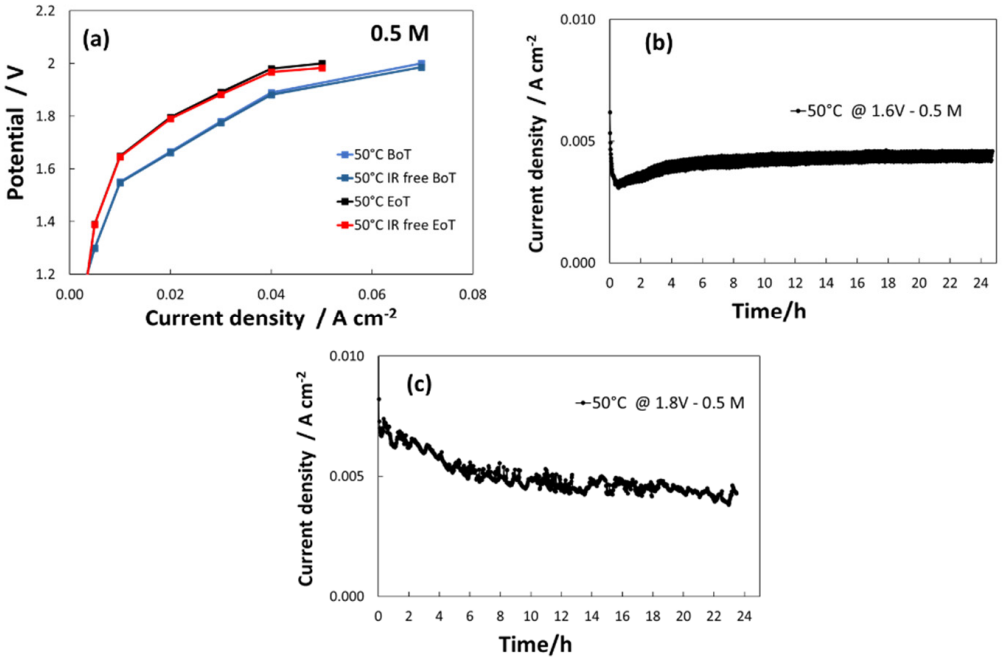

Figure 7. Polarization curves at 50 °C (**a**) CuOx/KB-Sustainion X37-50 -$NiFeO_x$/KB (BoT Rs = 0.32 Ohm cm^2 and EoT Rs = 0.2 Ohm cm^2) (**b**) chrono-amperometric curve at 1.6 V in presence of CO_2 in presence of 0.5 M $NaHCO_3$. (**c**) chrono-amperometric curve at 1.8 V in presence of CO_2 and in presence of 0.5 M $NaHCO_3$.

In Figure 8, the chromatograms of liquid phases analysis obtained at different potentials are reported. The presence of ethanol and methanol was observed mainly in 0.1 M of $NaHCO_3$. The product yields are specified in Table 1. According to the reactions 1 and 4

above reported, we calculated a Faradaic efficiency of approximately 5%. Consequently, the residual current was mainly involved in forming other undetected gas species.

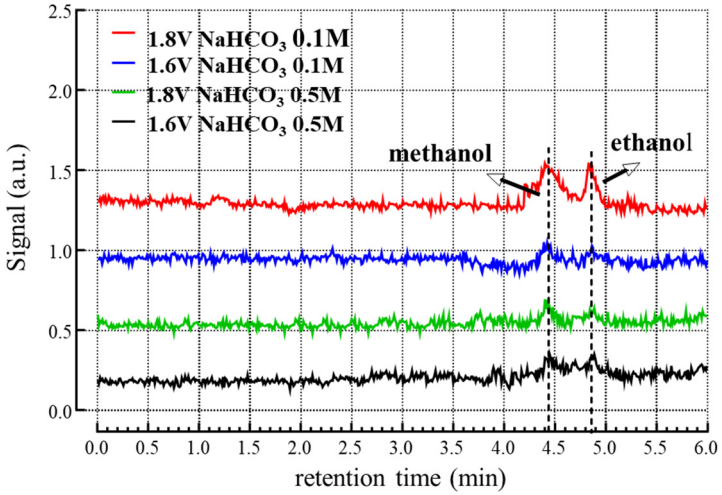

Figure 8. Liquid-phase analysis at the cathode outlet (CuOx/KB-Sustainion X37-50-NiFeO/KB), in the presence of 0.1 M and 0.5 M $NaHCO_3$ feed at different potentials.

The presence of two waves in the polarisation curves indicates that the two catalytic sites are effective in different potential ranges. For better accuracy, the results are reported in the potentiodynamic mode [6,41].

The catalytic activity of the CuO-Ag/KB was evaluated by electrochemical measurements (Figure 9a). Liquid-phase analysis at the cathode outlet in the presence of different electrolytes for the CO_2 reduction at Ag-CuO/KB catalyst is reported in Table 2. A higher current is achieved compared to CuOx in the initial experiment under similar conditions and lower deactivation after the steady-state potentiostatic test at 1.8 V in 0.1 M $NaHCO_3$. Methanol and ethanol were observed in the presence of 0.1M $NaHCO_3$. Thus, only ethanol was observed when KOH was recirculated at the anode of the cell (Figure 9b).

Table 2. Liquid-phase analysis for cell based on CuOxAg/KB-Sustainion X37-50-NiFeOx/KB.

CuOxAg/KB-Sustanion-NiFeOx/KB			
Operative Conditions	**Product Yield (μmol g_{cat}^{-1})**		**CO_2 Conversion Rate (μmol g_{cat}^{-1} h^{-1})**
	Methanol	**Ethanol**	
Cathode: CO_2 (50 °C) Anode: 0.1 M $NaHCO_3$; 24 h	34.7	7.5	2.07
CuOxAg/KB-Sustanion-NiFeOx/KB			
Operative Conditions	**Product Yield (μmol g_{cat}^{-1})**		**CO_2 Conversion Rate (μmol g_{cat}^{-1} h^{-1})**
	Methanol	**Ethanol**	
Cathode: CO_2 (50 °C) Anode: 1 M KOH; 22 h	0	5.45	0.52

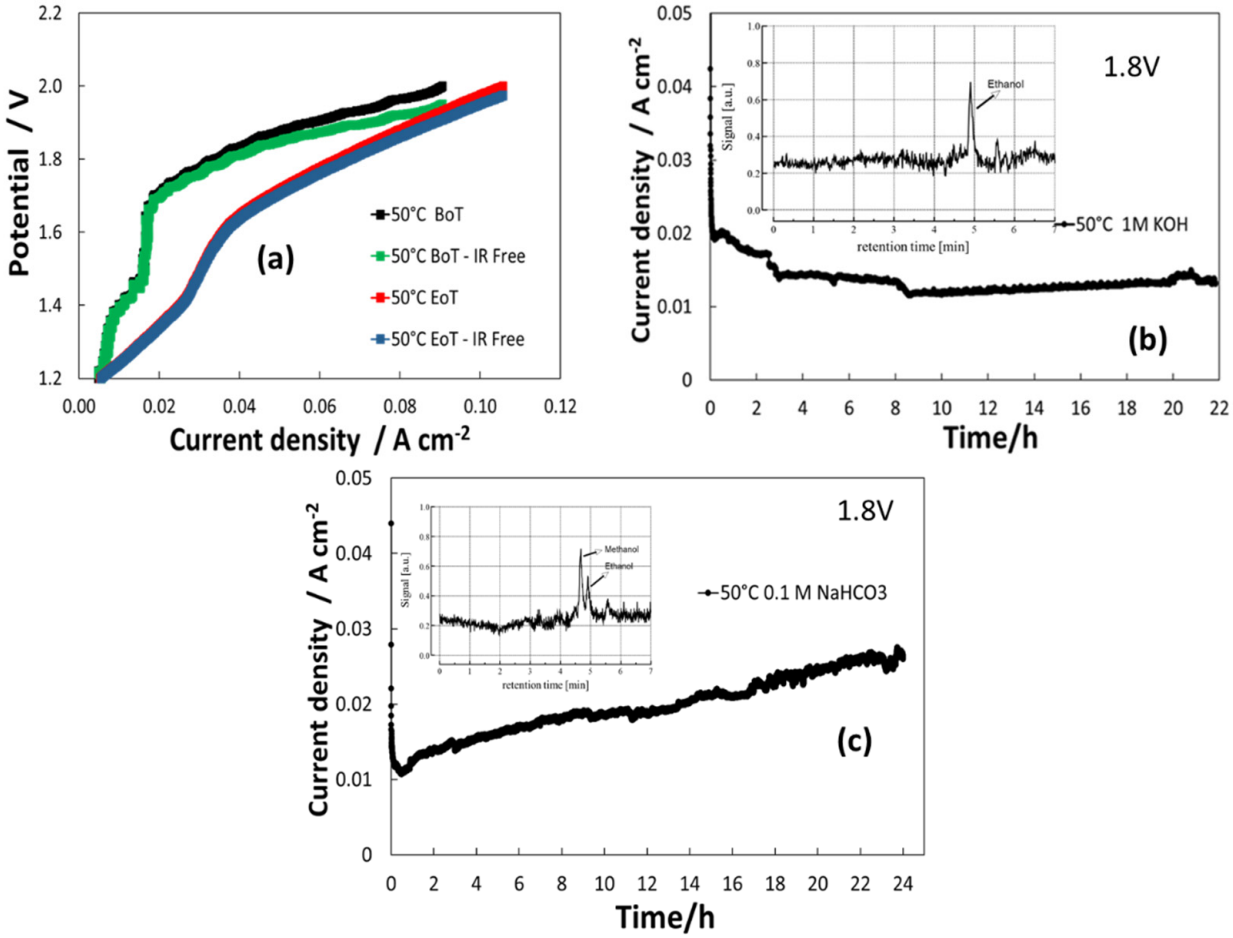

Figure 9. Polarization curves at 50 °C (**a**) CuOxAg/KB-Sustainion X37-50-NiFeO$_x$ KB (BoT Rs = 0.54 Ohm cm^2 and EoT Rs = 0.24 Ohm cm^{-2}). (**b**) Liquid-phase analysis at the cathode outlet, in the presence of 1M KOH at 1.8 V. (**c**) Liquid-phase analysis at the cathode outlet, in the presence of 0.1 M $NaHCO_3$ at 1.8 V.

The enhanced electrocatalytic CO_2 reduction activity of CuOxAg/KB catalyst compared to CuOx/KB can be attributed to the synergistic effects at the interface between Cu and Ag. Wanyu Su et al. investigated the Cu/Cu_2O-Ag-x for efficient electrochemical CO_2 reduction and found a synergetic role of Ag and CuO in the facilitation of C–C coupling reaction, thus boosting the selectivity towards the C^{2+} products [28]. The higher current density recorded in the CO_2 environment in the presence of 0.1 M $NaHCO_3$ at 1.8 V confirms that the CuOxAg/KB is electrocatalytically active for CO_2 reduction. Interestingly, after a durability test of only 24 h at 1.8 V, it was observed an increase of current up to 0.02 A cm^{-2}. The productivity of alcohols during the CO_2 reduction process is reported for two similar MEAs tested under different conditions in Table 2. The highest productivity was achieved for CuOxAg/KB in 0.1 M $NaHCO_3$. However, only ethanol and essential traces of methanol were obtained in KOH. Methanol was observed at 50 °C in the presence of $NaHCO_3$ with a yield larger than ethanol for the formulation CuO/KB [25,42–45]. Karapinar and coworkers, in their review, reported that the addition of a secondary metal in a copper-based catalytic system is a widely used approach to tune the electronic structure of Cu and the binding energy of the key intermediates formed during the CO_2 reduction and thereby improve the activity and selectivity for ethanol.

3. Material and Methods

3.1. Synthesis of Catalysts

Catalysts were prepared according to the oxalate method (Patent WO2004049491) [46]. Cu or Ag nitrates were dissolved in distilled water and mixed with a solution of oxalic acid neutralised at pH 6.5 with NaOH. The molar ratio between the chelating agent and metal was 10. A metal complex was formed and then decomposed at 80 °C with hydrogen peroxide to achieve a precipitate that then was filtered, washed and dried at 100 °C for 24 h. The raw powders were subsequently calcined at 350 °C for 120 min. The Ag catalyst was successively treated in diluted 5% H_2/95% He atmosphere to form metallic silver nanoparticles. Finally, the as-prepared CuO and Ag specimens were milled for 24 h at 160 rpm.

3.2. Physicochemical Characterisation

The preliminary physical–chemical characterisations of synthesised electrocatalyst consisted in the analyses of phases and size of crystallites using a Philips X-pert 3710 X-ray diffractometer (Panalytical Italia, Lissone, Italy) equipped with a Cu Kα radiation operating at 40 kV and 20 mA. A FEI XL 30 scanning electron microscope (SEM) (FEI, Eindhoven, The Netherlands) equipped with energy dispersive X-ray analysis (EDX) (FEI, Eindhoven, The Netherlands) was used to investigate the composition and morphology of the sample at a micrometric level. The morphology of catalysts at the nanoscale magnification was studied through the Transmission Electron Microscopy (TEM-FEI CM12 equipped with LaB6 filament) (FEI, Eindhoven, The Netherlands). X-ray photoelectron spectroscopy (XPS) evaluated the surface chemical composition of the samples and the chemical environment of each element. Spectra were recorded using a Physical Electronics GMBH PHI 5800-01 spectrometer (Physical Electronics GmbH, Munich, Germany), equipped with a monochromatic Al-Ka source (1486.6 eV) with a beam of 300 W.

The surface chemical composition of the samples and chemical environment were evaluated by X-ray photoelectron spectroscopy (XPS). Spectra were recorded using a Physical Electronics GMBH PHI 5800-01 spectrometer (Physical Electronics GmbH, Munich, Germany), equipped with a monochromatic Al-Ka source (1486.6 eV) with a power beam of 300 W. The pass energy for determination of the oxidation state and concentration of surface species was 11.0 eV and 58.0 eV, respectively. The BE regions of C1s (280–300 eV), Cu2p (920–968 eV), Ag3d (364–378 eV) and O1s (525–535 eV) were investigated, taking the C1s line (284.8 eV) of adventitious carbon as reference, as reported in the literature [47].

3.3. Electrochemical Characterisation

Concerning the membrane electrode assemblies (MEAs), the first step was to prepare the anode and cathode inks to be deposited on backing layers and successively assembled with the electrolyte. The anode used in all electrochemical experiments was the NiFeOx electrocatalyst, fully described in our previous paper [46]. The inks contained 33 wt.% of anionic ionomer and 67 wt. % of electrocatalyst. These were dispersed and were sonicated for 30 min in ethanol before manufacturing the related electrodes. The gas diffusion layer (GDL) used for the cathode and anode was a backing layer purchased by Spectracarb, which was spray-coated with the ink of each electrocatalyst [48]. This procedure was conducted on a heated plate to facilitate the evaporation of ethanol. According to this procedure, the total metal loaded in the final electrodes was 2.5 mg cm^{-2} for the anode and 3 mg cm^{-2} for the CuO and CuO-Ag cathode [49,50], which were the subject of this study. Finally, cold-pressed membrane–electrode assemblies (MEAs) with a geometrical area of 5 cm^2 for both electrodes were manufactured. The polymer electrolyte used was a Sustainion® X37-50 anion exchange membrane. The MEAs were then assembled in a nickel housing in single-cell configuration, and temperature-controlled in the range 30–50 °C for the time required by the electrochemical experiments. During the experiments, $NaHCO_3$ (0.1 M or 0.5 M) or KOH solution (1 M) was recirculated at the anode side compartment at a flow rate of 4 mL min^{-1} using a peristaltic pump. Humidified CO_2 was preheated at the cell temperature and then fed to the cathode compartment at a flow rate of 50 mL

min^{-1}. The electrochemical investigations consisted of polarisation curves (cell potential versus current density) and chronoamperometry analysis. The Keithley as power supply system (Tektronic, Rome, Italy) was used. The series resistance (Rs) was determined using an impedance bridge (4338B, Agilent, Rome, Italy) at a frequency of 1 kHz. Further tests consisted of the gas chromatographic analysis for the cathodic outlet collected during the endurance tests to check any possible organic soluble species. The liquid was entrapped in a vial maintained at temperatures below 0 °C into a cryogenic apparatus to comply with this.

A GC model Agilent 7890 A was used for this scope. The instrument included a capillary column (30 m × 0.53 mm × 0.2 µm film thickness) model Supelcowax 10 (Merck KGaA, Darmstadt, Germany), directly connected to a flame ionization detector. The analytes were eluted using helium as carrier gas. Each compound's "sensitive factors" were determined by calibrating the GC with standards.

4. Conclusions

This work deals with a screening of cathode electrocatalysts in a coelectrolysis cell involving conversion of CO_2 and water to sustainable fuels. NonCRM electrocatalysts were developed and assessed in terms of performance, productivity to alcohols, selectivity, and activity. Using the CuO/KB and CuO-Ag/KB composite catalysts, alcohols such as methanol and ethanol were obtained at both 1.6 and 1.8 V in 0.1 M $NaHCO_3$ recirculated at the anode. By using a CuO/KB catalyst, a methanol and ethanol yield of 29.5 µmol/g_{cat} and 14.4 µmol/g_{cat} were obtained, respectively, in a 24 h test at 1.8 V, whereas 34.65 µmol/g_{cat} of methanol and 7.45 µmol/g_{cat} of ethanol was achieved for CuOAg/KB at the same potential during 24 h operation. These results appear very promising for alternative and innovative green fuels production from CO_2 conversion.

Author Contributions: S.C.Z.: conceptualization, investigation, methodology, visualisation, writing—original draft, revision draft, validation. M.L.F.: investigation, methodology, visualization, data curation. A.P.: investigation, methodology, revision draft. L.S.: investigation, methodology. S.T.: investigation, methodology, data curation, revision draft. C.L.V.: investigation, revision draft. A.S.A.: conceptualization, supervision, writing—review and editing, funding acquisition. All authors have read and agreed to the published version of the manuscript.

Funding: This research was funded by the EU H2020 LOTERCO2M project "CRM-free Low Temperature Electrochemical Reduction of CO_2 to Methanol" Grant Agreement number: 761093.

Data Availability Statement: Not applicable.

Conflicts of Interest: The authors declare no conflict of interest.

References

1. Kuhl, K.P.; Hatsukade, T.; Cave, E.R.; Abram, D.N.; Kibsgaard, J.; Jaramillo, T.F. Electrocatalytic Conversion of Carbon Dioxide to Methane and Methanol on Transition Metal Surfaces. *J. Am. Chem. Soc.* **2014**, *136*, 14107–14113. [CrossRef] [PubMed]
2. Zhang, W.; Hu, Y.; Ma, L.; Zhu, G.; Wang, Y.; Xue, X.; Chen, R.; Yang, S.; Jin, Z. Progress and Perspective of Electrocatalytic CO_2 Reduction for Renewable Carbonaceous Fuels and Chemicals. *Adv. Sci.* **2018**, *5*, 1700275. [CrossRef]
3. Küngas, R. Review—Electrochemical CO_2 Reduction for CO Production: Comparison of Low- and High-Temperature Electrolysis Technologies. *J. Electrochem. Soc.* **2020**, *167*, 044508. [CrossRef]
4. Trocino, S.; Vecchio, C.L.; Zignani, S.C.; Carbone, A.; Saccà, A.; Baglio, V.; Gómez, R.; Aricò, A.S. Dry Hydrogen Production in a Tandem Critical Raw Material-Free Water Photoelectrolysis Cell Using a Hydrophobic Gas-Diffusion Backing Layer. *Catalysts* **2020**, *10*, 1319. [CrossRef]
5. Qi, Z.; Biener, M.M.; Kashi, A.R.; Hunegnaw, S.; Leung, A.; Ma, S.; Huo, Z.; Kuhl, K.P.; Biener, J. Scalable Fabrication of High Activity Nanoporous Copper Powders for Electrochemical CO_2 Reduction via Ball Milling and Dealloying. *J. CO_2 Util.* **2021**, *45*, 101454. [CrossRef]
6. Marques da Silva, A.; Raaijman, S.; Santana, C.; Assaf, J.; Gomes, J.F.; Koper, M. Reprint of "Electrocatalytic CO_2 Reduction to C2+ Products on Cu and CuxZny Electrodes: Effects of Chemical Composition and Surface Morphology". *J. Electroanal. Chem.* **2021**, *896*, 115609. [CrossRef]
7. Ali, S.; Razzaq, A.; Kim, H.; In, S.-I. Activity, Selectivity, and Stability of Earth-Abundant CuO/Cu_2O/Cu0-Based Photocatalysts toward CO_2 Reduction. *Chem. Eng. J.* **2022**, *429*, 131579. [CrossRef]

8. Zeng, L.; Shi, J.; Chen, H.; Lin, C. Ag Nanowires/C as a Selective and Efficient Catalyst for CO_2 Electroreduction. *Energies* **2021**, *14*, 2840. [CrossRef]
9. Qiao, J.; Liu, Y.; Hong, F.; Zhang, J. A Review of Catalysts for the Electroreduction of Carbon Dioxide to Produce Low-Carbon Fuels. *Chem. Soc. Rev.* **2014**, *43*, 631–675. [CrossRef]
10. Rabinowitz, J.A.; Kanan, M.W. The Future of Low-Temperature Carbon Dioxide Electrolysis Depends on Solving One Basic Problem. *Nat. Commun.* **2020**, *11*, 5231. [CrossRef]
11. Song, J.T.; Song, H.; Kim, B.; Oh, J. Towards Higher Rate Electrochemical CO_2 Conversion: From Liquid-Phase to Gas-Phase Systems. *Catalysts* **2019**, *9*, 224. [CrossRef]
12. Kondratenko, E.V.; Mul, G.; Baltrusaitis, J.; Larrazábal, G.O.; Pérez-Ramírez, J. Status and Perspectives of CO_2 Conversion into Fuels and Chemicals by Catalytic, Photocatalytic and Electrocatalytic Processes. *Energy Environ. Sci.* **2013**, *6*, 3112–3135. [CrossRef]
13. Yin, Z.; Peng, H.; Wei, X.; Zhou, H.; Gong, J.; Huai, M.; Xiao, L.; Wang, G.; Lu, J.; Zhuang, L. An Alkaline Polymer Electrolyte CO_2 Electrolyzer Operated with Pure Water. *Energy Environ. Sci.* **2019**, *12*, 2455–2462. [CrossRef]
14. Kaczur, J.J.; Yang, H.; Liu, Z.; Sajjad, S.D.; Masel, R.I. Carbon Dioxide and Water Electrolysis Using New Alkaline Stable Anion Membranes. *Front. Chem.* **2018**, *6*, 263. [CrossRef] [PubMed]
15. Cho, M.K.; Park, H.-Y.; Lee, H.J.; Kim, H.-J.; Lim, A.; Henkensmeier, D.; Yoo, S.J.; Kim, J.Y.; Lee, S.Y.; Park, H.S.; et al. Alkaline Anion Exchange Membrane Water Electrolysis: Effects of Electrolyte Feed Method and Electrode Binder Content. *J. Power Sources* **2018**, *382*, 22–29. [CrossRef]
16. Kutz, R.B.; Chen, Q.; Yang, H.; Sajjad, S.D.; Liu, Z.; Masel, I.R. Sustainion Imidazolium-Functionalized Polymers for Carbon Dioxide Electrolysis. *Energy Technol.* **2017**, *5*, 929–936. [CrossRef]
17. Sebastián, D.; Palella, A.; Baglio, V.; Spadaro, L.; Siracusano, S.; Negro, P.; Niccoli, F.; Aricò, A. CO_2 Reduction to Alcohols in a Polymer Electrolyte Membrane Co-Electrolysis Cell Operating at Low Potentials. *Electrochim. Acta* **2017**, *241*, 28–40. [CrossRef]
18. Manabe, A.; Kashiwase, M.; Hashimoto, T.; Hayashida, T.; Kato, A.; Hirao, K.; Shimomura, I.; Nagashima, I. Basic Study of Alkaline Water Electrolysis. *Electrochim. Acta* **2013**, *100*, 249–256. [CrossRef]
19. Lee, S.; Ocon, J.D.; Son, Y.; Lee, J. Alkaline CO_2 Electrolysis toward Selective and Continuous HCOO– Production over SnO_2 Nanocatalysts. *J. Phys. Chem. C* **2015**, *119*, 4884–4890. [CrossRef]
20. Zhang, L.; Merino-Garcia, I.; Albo, J.; Sánchez-Sánchez, C.M. Electrochemical CO_2 Reduction Reaction on Cost-Effective Oxide-Derived Copper and Transition Metal–Nitrogen–Carbon Catalysts. *Electrocatal. Sens. Biosens.* **2020**, *23*, 65–73. [CrossRef]
21. Krause, K.; Lee, C.; Lee, J.; Fahy, K.; Shafaque, H.; Kim, P.; Shrestha, P.; Bazylak, A. Unstable Cathode Potential in Alkaline Flow Cells for CO_2 Electroreduction Driven by Gas Evolution. *ACS Sustain. Chem. Eng.* **2021**, *9*, 5570–5579. [CrossRef]
22. Roy, A.; Jadhav, H.; Park, S.J.; Seo, J. Recent Advances in the Possible Electrocatalysts for the Electrochemical Reduction of Carbon Dioxide into Methanol. *J. Alloys Compd.* **2021**, *887*, 161449. [CrossRef]
23. Schizodimou, A.; Kyriacou, G. Acceleration of the Reduction of Carbon Dioxide in the Presence of Multivalent Cations. *Electrochim. Acta* **2012**, *78*, 171–176. [CrossRef]
24. Albo, J.; Sáez, A.; Solla-Gullón, J.; Montiel, V.; Irabien, A. Production of Methanol from CO_2 Electroreduction at Cu_2O and Cu_2O/ZnO-Based Electrodes in Aqueous Solution. *Appl. Catal. B Environ.* **2015**, *176–177*, 709–717. [CrossRef]
25. Peterson, A.A.; Abild-Pedersen, F.; Studt, F.; Rossmeisl, J.; Nørskov, J.K. How Copper Catalyzes the Electroreduction of Carbon Dioxide into Hydrocarbon Fuels. *Energy Environ. Sci.* **2010**, *3*, 1311–1315. [CrossRef]
26. Wang, X.; Klingan, K.; Klingenhof, M.; Möller, T.; Ferreira de Araújo, J.; Martens, I.; Bagger, A.; Jiang, S.; Rossmeisl, J.; Dau, H.; et al. Morphology and Mechanism of Highly Selective Cu(II) Oxide Nanosheet Catalysts for Carbon Dioxide Electroreduction. *Nat. Commun.* **2021**, *12*, 794. [CrossRef]
27. Shu, D.; Wang, M.; Tian, F.; Zhang, H.; Peng, C. A Dual-Cathode Study on Ag-Cu Sequential CO_2 Electroreduction towards Hydrocarbons. *J. CO_2 Util.* **2021**, *45*, 101444. [CrossRef]
28. Su, W.; Ma, L.; Cheng, Q.; Wen, K.; Wang, P.; Hu, W.; Zou, L.; Fang, J.; Yang, H. Highly Dispersive Trace Silver Decorated Cu/Cu_2O Composites Boosting Electrochemical CO_2 Reduction to Ethanol. *J. CO_2 Util.* **2021**, *52*, 101698. [CrossRef]
29. Monteiro, M.C.O.; Philips, M.F.; Schouten, K.J.P.; Koper, M.T.M. Efficiency and Selectivity of CO_2 Reduction to CO on Gold Gas Diffusion Electrodes in Acidic Media. *Nat. Commun.* **2021**, *12*, 4943. [CrossRef]
30. Ting, L.R.L.; García-Muelas, R.; Martín, A.J.; Veenstra, F.L.P.; Chen, S.T.-J.; Peng, Y.; Per, E.Y.X.; Pablo-García, S.; López, N.; Pérez-Ramírez, J.; et al. Electrochemical Reduction of Carbon Dioxide to 1-Butanol on Oxide-Derived Copper. *Angew. Chem. Int. Ed.* **2020**, *59*, 21072–21079. [CrossRef]
31. Ma, M.; Clark, E.L.; Therkildsen, K.T.; Dalsgaard, S.; Chorkendorff, I.; Seger, B. Insights into the Carbon Balance for CO_2 Electroreduction on Cu Using Gas Diffusion Electrode Reactor Designs. *Energy Environ. Sci.* **2020**, *13*, 977–985. [CrossRef]
32. Zhang, S.-Y.; Li, T.-T.; Zhu, H.-L.; Zheng, Y.-Q. Co_3O_4 Polyhedrons with Enhanced Electric Conductivity as Efficient Water Oxidation Electrocatalysts in Alkaline Medium. *J. Mater. Sci.* **2018**, *53*, 4323–4333. [CrossRef]
33. Lo Vecchio, C.; Trocino, S.; Giacoppo, G.; Barbera, O.; Baglio, V.; Díez-García, M.I.; Contreras, M.; Gómez, R.; Aricò, A.S. Water Splitting with Enhanced Efficiency Using a Nickel-Based Co-Catalyst at a Cupric Oxide Photocathode. *Catalysts* **2021**, *11*, 1363. [CrossRef]
34. Zhao, J.; Xue, S.; Barber, J.; Zhou, Y.; Meng, J.; Ke, X. An Overview of Cu-Based Heterogeneous Electrocatalysts for CO_2 Reduction. *J. Mater. Chem. A* **2020**, *8*, 4700–4734. [CrossRef]

35. Spadaro, L.; Palella, A.; Arena, F. Copper-Iron-Zinc-Cerium Oxide Compositions as Most Suitable Catalytic Materials for the Synthesis of Green Fuels via CO_2 Hydrogenation. *Proc. V Int. Conf. Catal. Renew. Sources Fuel Energy Chem.* **2021**, *379*, 230–239. [CrossRef]
36. Crisafulli, R.; Barros, V.; Oliveira, F.; Rocha, T.; Zignani, S.; Spadaro, L.; Palella, A.; Dias, J.; Linares Leon, J. On the Promotional Effect of Cu on Pt for Hydrazine Electrooxidation in Alkaline Medium. *Appl. Catal. B Environ.* **2018**, *236*, 36–44. [CrossRef]
37. Spadaro, L.; Palella, A.; Arena, F. Totally-Green Fuels via CO_2 Hydrogenation. *Bull. Chem. React. Eng. Catal.* **2020**, *15*, 390–404. [CrossRef]
38. Corro, G.; Vidal, E.; Cebada, S.; Pal, U.; Bañuelos, F.; Vargas, D.; Guilleminot, E. Electronic State of Silver in Ag/SiO_2 and Ag/ZnO Catalysts and Its Effect on Diesel Particulate Matter Oxidation: An XPS Study. *Appl. Catal. B Environ.* **2017**, *216*, 1–10. [CrossRef]
39. Barbera, K.; Frusteri, L.; Italiano, G.; Spadaro, L.; Frusteri, F.; Perathoner, S.; Centi, G. Low-temperature graphitization of amorphous carbon nanospheres. *Chin. J. Catal.* **2014**, *35*, 869–876. [CrossRef]
40. Pantea, D.; Darmstadt, H.; Kaliaguine, S.; Roy, C. Electrical Conductivity of Conductive Carbon Blacks: Influence of Surface Chemistry and Topology. *Appl. Surf. Sci.* **2003**, *217*, 181–193. [CrossRef]
41. Benson, E.E.; Kubiak, C.P.; Sathrum, A.J.; Smieja, J.M. Electrocatalytic and Homogeneous Approaches to Conversion of CO_2 to Liquid Fuels. *Chem. Soc. Rev.* **2009**, *38*, 89–99. [CrossRef] [PubMed]
42. Vickers, J.W.; Alfonso, D.; Kauffman, D.R. Electrochemical Carbon Dioxide Reduction at Nanostructured Gold, Copper, and Alloy Materials. *Energy Technol.* **2017**, *5*, 775–795. [CrossRef]
43. Salehi-Khojin, A.; Jhong, H.-R.M.; Rosen, B.A.; Zhu, W.; Ma, S.; Kenis, P.J.A.; Masel, R.I. Nanoparticle Silver Catalysts That Show Enhanced Activity for Carbon Dioxide Electrolysis. *J. Phys. Chem. C* **2013**, *117*, 1627–1632. [CrossRef]
44. Calvinho, K.U.D.; Laursen, A.B.; Yap, K.M.K.; Goetjen, T.A.; Hwang, S.; Murali, N.; Mejia-Sosa, B.; Lubarski, A.; Teeluck, K.M.; Hall, E.S.; et al. Selective CO_2 Reduction to C_3 and C_4 Oxyhydrocarbons on Nickel Phosphides at Overpotentials as Low as 10 MV. *Energy Environ. Sci.* **2018**, *11*, 2550–2559. [CrossRef]
45. Karapinar, D.; Creissen, C.E.; Rivera de la Cruz, J.G.; Schreiber, M.W.; Fontecave, M. Electrochemical CO_2 Reduction to Ethanol with Copper-Based Catalysts. *ACS Energy Lett.* **2021**, *6*, 694–706. [CrossRef]
46. Campagna Zignani, S.; Lo Faro, M.; Trocino, S.; Aricò, A.S. Investigation of NiFe-Based Catalysts for Oxygen Evolution in Anion-Exchange Membrane Electrolysis. *Energies* **2020**, *13*, 1720. [CrossRef]
47. Arena, F.; Trunfio, G.; Negro, J.; Spadaro, L. Synthesis of Highly Dispersed MnCeOx Catalysts via a Novel "Redox-Precipitation" Route. *Mater. Res. Bull.* **2008**, *43*, 539–545. [CrossRef]
48. Erkan, S.; Eroglu, I. Progress in Clean Energy. In *Ultrasonic Spray Coating Technique for High-Performance PEM Fuel Cell Electrode Manufacturing*; Dincer, I., Colpan, C., Kizilkan, O., Ezan, M., Eds.; Springer: Cham, Switzerland, 2015; Volume 2. [CrossRef]
49. Zhu, Q.; Sun, X.; Yang, D.; Ma, J.; Kang, X.; Zheng, L.; Zhang, J.; Wu, Z.; Han, B. Carbon Dioxide Electroreduction to C2 Products over Copper-Cuprous Oxide Derived from Electrosynthesized Copper Complex. *Nat. Commun.* **2019**, *10*, 3851. [CrossRef]
50. Kim, D.; Kley, C.S.; Li, Y.; Yang, P. Copper Nanoparticle Ensembles for Selective Electroreduction of CO_2 to C_2–C_3 Products. *Proc. Natl. Acad. Sci. USA* **2017**, *114*, 10560. [CrossRef]